ADVANCED SCIENCE Open Access
www.advancedscience.com

Embracing Defects and Disorder in Magnetic Nanoparticles

Aidin Lak, Sabrina Disch,* and Philipp Bender**

Iron oxide nanoparticles have tremendous scientific and technological potential in a broad range of technologies, from energy applications to biomedicine. To improve their performance, single-crystalline and defect-free nanoparticles have thus far been aspired. However, in several recent studies, defect-rich nanoparticles outperform their defect-free counterparts in magnetic hyperthermia and magnetic particle imaging (MPI). Here, an overview on the state-of-the-art of design and characterization of defects and resulting spin disorder in magnetic nanoparticles is presented with a focus on iron oxide nanoparticles. The beneficial impact of defects and disorder on intracellular magnetic hyperthermia performance of magnetic nanoparticles for drug delivery and cancer therapy is emphasized. Defect-engineering in iron oxide nanoparticles emerges to become an alternative approach to tailor their magnetic properties for biomedicine, as it is already common practice in established systems such as semiconductors and emerging fields including perovskite solar cells. Finally, perspectives and thoughts are given on how to deliberately induce defects in iron oxide nanoparticles and their potential implications for magnetic tracers to monitor cell therapy and immunotherapy by MPI.

1. Introduction

Despite their common negative connotation, defects and disorder can be highly desirable in nature and materials design.[1] Colorful examples for nature's design-by-disorder are butterfly wings, whose vibrant colors originate from slightly disordered arrangements of photonic crystals,[2] and white beetle scales, whose exceptional whiteness is caused by a very high degree of disorder.[3] Having learned from nature, mimicking its powerful design-by-disorder strategy has become an emerging field of research in materials science.[4] This design method has led to novel applications, for example, within the field of disordered photonics.[5] Nowadays, defect-engineering is commonly used in designing semiconductors,[6] perovskite solar cells,[7] metals,[8] multiferroics,[9] nanocomposites,[10] and carbon materials[11,12] to tailor functional properties. Recent years have witnessed ground-breaking work in this area,[13–16] focusing exclusively on exploiting structural disorder in various functional materials such as metal–organic frameworks to optimize specific material characteristics. Notably, the electronic structure of condensed matter is significantly affected by intrinsic defects such as vacancies, impurities, and dislocations,[17] which in turn modify macroscopic material characteristics, including optical[18] and magnetic properties, for example, by domain wall pinning.[19]

However, for magnetic materials changing our negative perception about defects has had a much slower pace than other fields. Recently, the generic relevance of the defect-induced Dzyaloshinskii–Moriya interaction for the spin microstructure of defect-rich ferromagnets was verified,[20] suggesting a potential for creation of local chiral spin textures, that is, skyrmions,[21] in all kinds of disordered magnetic materials. Magnetic materials offer wide-spread novel technological potential,[22] with magnetic nanoparticles,[23] especially iron oxide nanoparticles, being indispensable candidates for varieties of biomedical applications,[24] including magnetic hyperthermia[25] and magnetic particle and resonance imaging (MPI,[26] MRI[27]).

To assess and optimize the performance of magnetic nanoparticles, it is crucial to consider their structure and magnetism on a variety of length scales, ranging from the atomistic to the macroscopic regime (**Figure 1**). While considering magnetic nanoparticles as mesoscale dipoles is sufficient to understand the qualitative principle of magnetic hyperthermia and MPI, the internal MNP structure directly impacts magnetic properties and, hence, magnetic hyperthermia and MPI performance. Due to their large surface to volume ratio, magnetic nanoparticles are particularly prone to structural and compositional defects,[28] and thus

Dr. A. Lak
Department of Physics and Center for NanoScience
LMU Munich
Amalienstr. 54, Munich 80799, Germany
E-mail: lak.aidin@lmu.de
Dr. S. Disch
Department für Chemie
Universität zu Köln
Greinstraße 4-6 Köln 50939, Germany
E-mail: sabrina.disch@uni-koeln.de
Dr. P. Bender[+]
Department of Physics and Materials Science
University of Luxembourg
162A avenue de la Faïencerie Luxembourg L-1511, Grand Duchy of Luxembourg
E-mail: philipp.bender@uni.lu

The ORCID identification number(s) for the author(s) of this article can be found under https://doi.org/10.1002/advs.202002682

[+]Present address: Heinz Maier-Leibnitz Zentrum (MLZ), Technische Universität München, D-85748 Garching, Germany

DOI: 10.1002/advs.202002682

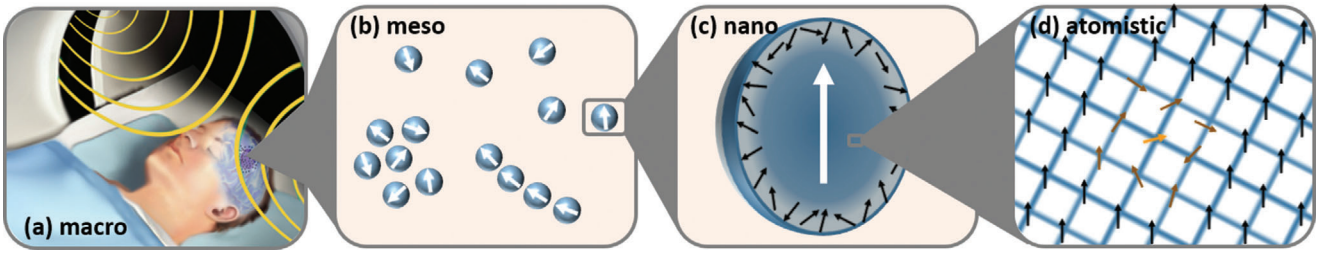

Figure 1. Multiple length scales in magnetic nanoparticles. a) The macroscopic application (here: magnetic hyperthermia for the treatment of glioblastoma) can be understood qualitatively by considering magnetic nanoparticles b) on the mesoscale as magnetic dipoles of the respective bulk material with nanosized dimensions. Quantitatively, magnetic nanoparticles performance is critically affected by spin disorder on both c) the nanoscale (i.e., its distribution within the particle from surface into the particle interior) and d) the atomic scale (e.g., site-defect induced spin disorder). As shown, for example, in ref. [63], defects in the crystalline structure cause atomistic spin disorder that can critically modify the magnetic properties of nanoparticles and hence influence the macroscopic ensemble properties and therefore their magnetic hyperthermia performance. a) Adapted under terms of the CC-BY licence.[45] Copyright 2014, The Authors, published by Frontiers.

synthesis of defect-free magnetic nanoparticles remains highly challenging.[29] From very early aqueous synthesis of iron oxide nanoparticle suspensions through a co-precipitation method,[30] there have been enormous efforts on controlling physicochemical properties, often with the goal to prepare single-crystalline iron oxide nanoparticles.[31] To date, the synthesis of defect-free iron oxide nanoparticles remains the golden standard in colloidal chemistry.

Recently, however, it was demonstrated that in case of magnetic hyperthermia (and also MPI, MRI) defect-rich iron oxide nanoparticles can actually outperform their defect-free counterparts.[32–39] Motivated by these striking results, here, we will remove the common stigma of defects in iron oxide nanoparticles. At first, we discuss recent studies on positive impacts of defects and disorder on magnetic hyperthermia performance of iron oxide nanoparticles. Next, we review the magnetic spin disorder in iron oxide nanoparticles associated with defects and disorder. Finally, we present an overview about the state-of-the-art on how to incorporate and induce defects in iron oxide nanoparticles.

2. Iron Oxide Nanoparticles in Biomedicine

2.1. Designing the Ideal Iron Oxide Nanoparticles for Magnetic Hyperthermia

Iron oxide nanoparticles transduce magnetic energy to heat through magnetic losses when exposed to external alternating magnetic fields. They can therefore serve as remotely activated, nanometric heat sources[40] to eradicate cancer cells after being intracellularly engulfed.[25,41] Remarkably, the concept of exploiting iron oxide nanoparticles as local heat sources has been recently expanded to other technologies such as catalysis,[42] water electrolysis,[43] and local polymerization.[44]

Magnetic hyperthermia is especially attractive for the treatment of inoperable tumors such as glioblastoma (illustrated in Figure 1a), the most common and a highly aggressive brain cancer.[45] Although magnetic hyperthermia is not yet a routine treatment, clinical trials are ongoing. With the clinical application of magnetic hyperthermia in mind, the following restrictions need to be considered regarding particle design to optimize the heating:[46] 1) focus on biocompatibility[47] and biodegradation: iron oxide nanoparticles are hitherto the only clinically approved heat transducers to be administered to humans;[48] 2) focus on Néel relaxation: iron oxide nanoparticles have to preserve their heating performance when intracellularly immobilized, as in the cellular milieu a physical rotation of nanoparticles, that is, Brownian relaxation, is mostly inhibited;[49–51] 3) focus on high-frequency and low-amplitude alternating fields: intracellularly immobilized iron oxide nanoparticles should induce hyperthermic effects, that is, rising temperature to ≈42 °C, but also comply with the biological safety limits.[52] Currently, most magnetic hyperthermia devices approved for clinical trials apply magnetic fields within a frequency range of 0.05–1.2 MHz and an amplitude range of 0–5 kA m^{-1} (although in some clinical trials amplitudes of up to 18 kA m^{-1} are used).[53]

The macroscopic heating power of an iron oxide nanoparticle ensemble is usually given by the specific absorption rate $SAR = f \cdot S/c$, where $S = \mu_0 \oint M(H)dH$ is the area of alternating field hysteresis loops, and c is the weight concentration of the magnetic material.[54] To better compare results from different experimental setups, the intrinsic loss parameter ILP was introduced, which is given by $ILP = SAR/(\mu_0 H_0^2 f)$.[55,56] Within the framework of the linear response theory, that is, at first approximation valid in case of low amplitudes, the ILP is given by $ILP = \pi\mu_0\chi''(\omega)/c$, where $\chi''(\omega)$ is the imaginary part of the complex ac-susceptibility.[57] It has been shown that in case of single-crystalline maghemite, when dispersed in highly viscous media, 14 nm nanoparticles exhibit the maximum heating performance at the frequency and field amplitude of 1000 kHz and 24.8 kA m^{-1}.[58] The heating behavior of nanoparticles can be largely influenced by mesoscale ensemble effects such as arrangement,[59] interactions,[60] and alignment.[61,62] Additionally, deviation from the perfect single-crystalline structure can affect particles magnetization and thus their magnetic heating. In case of small particles (i.e., smaller than ≈14 nm), a defect-induced magnetic hardening can be useful to improve their heating performance. Recently, Lappas et al.[63] observed that the magnetic heating of 10 nm iron oxide nanoparticles is increased by structural point defects inside the crystal lattice (sketch in Figure 1d). In this case, the improved heating compared to defect-free particles is explained by increased effective magnetic energy barrier KV thanks to individual point defects.

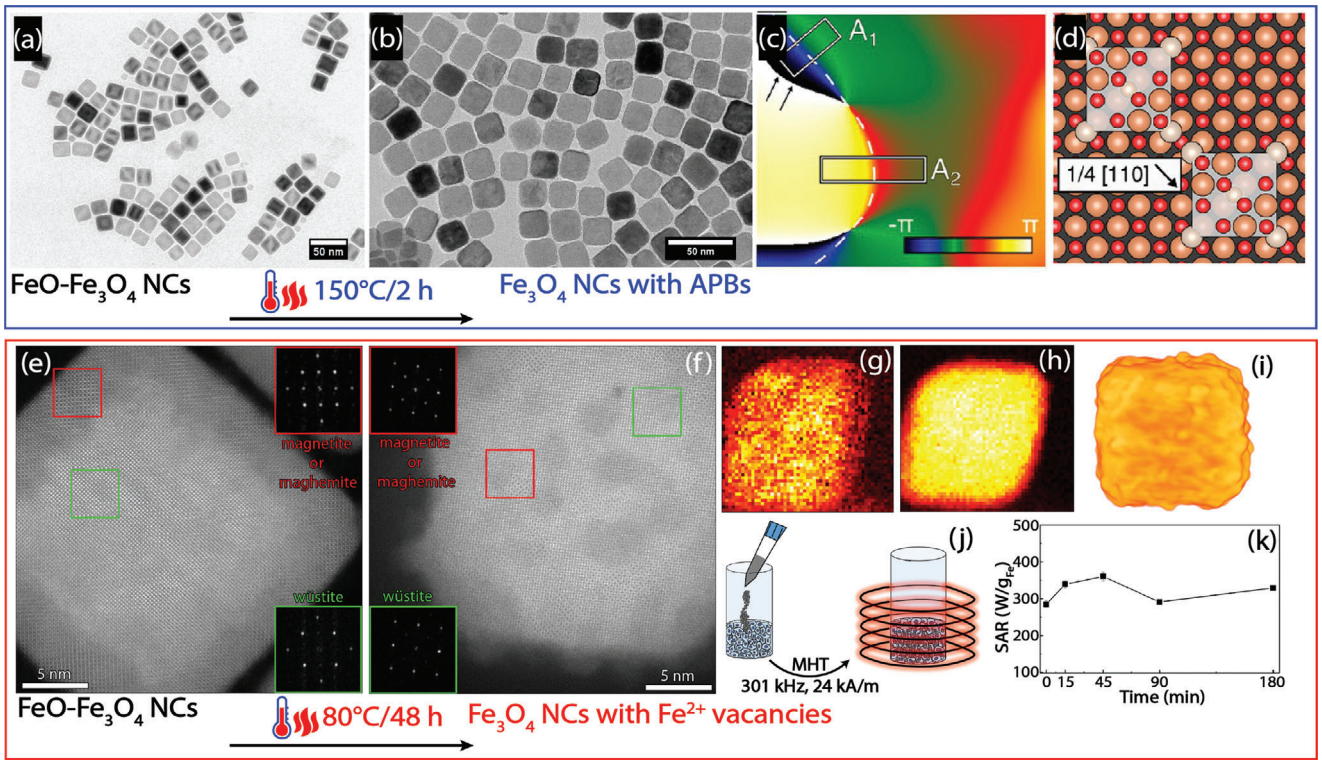

Figure 2. Thermally induced antiphase boundary (APB) defects and cation vacancies in iron oxide nanocubes synthesized via thermal decomposition of iron-oleate. Low-resolution TEM images of a) as-prepared FeO-Fe_3O_4 core–shell nanocubes and b) thermally annealed nanocubes at 150 °C for 2 h. c) Phase map of {220} spinel-exclusive fringe of a Fourier-filtered HRTEM image of a single particle acquired by geometric phase analysis (GPA), indicating an APB with the dashed line that is formed where two growing magnetite sub-domains coalescent. d) Scheme of unit cells of two Fe_3O_4 domains (white rectangulars) nucleated on an ideal FeO surface that are shifted by 1/4 [110]. Adapted with permission.[74] Copyright 2013, American Chemical Society. e) High-resolution HAADF-STEM image of an FeO-Fe_3O_4 core–shell nanocube: insets are Fourier analysis diffraction patterns of regions containing FeO and magnetite/maghemite. f) High-resolution HAADF-STEM image of a nanocube after 48 h annealing at 80 °C: insets are Fourier analysis diffraction patterns of regions containing FeO and magnetite/maghemite. g) Fe^{2+} and h) Fe^{3+} valency maps of a single thermally treated nanocube obtained by fitting the electron energy loss spectra of each pixel to the reference spectra. i) 3D visualization of the individual nanocube shown in (f), which was reconstructed using electron tomography technique. j) Scheme of evaluating in vitro magnetic hyperthermia performance of thermally treated nanoparticles during interaction and uptake by IGROV-1 breast cancer cells. k) Evolution of SAR values as a function of the incubation time were measured at field frequency and amplitude of 301 kHz and 24 kA m^{-1}. The SAR is virtually independent of nanoparticle cell internalization and immobilization. Adapted with permission.[37] Copyright 2018, American Chemical Society.

In case of large nanoparticles (larger than ≈14 nm), however, an increased KV would result in a complete blocking of the particle moments and thus eliminating the contribution of Néel relaxation in the magnetic heating. In this situation, on the one hand, driving field amplitudes above the coercive field are necessary to heat up the particles,[64] that is, fields much larger than 18 kA m^{-1}. On the other hand, to achieve an effective magnetic heating, large effective particle moments would be beneficial, which in turn implies large particle volumes. Clearly, large particles have counteracting effects on the overall magnetic hyperthermia. For this reason, we propose the use of large and magnetically soft iron oxide nanoparticles, so that they have an appreciable response $\chi''(\omega)$ at low field amplitudes.

A possible approach to reduce the effective anisotropy KV, and hence increase the initial susceptibility, is the introduction of structural defects. Planar defects such as grain boundaries, stacking faults, and twinning, and linear defects like edge and screw dislocations as well as point defects can cause the aforementioned defect-induced magnetic softening. This approach is well established for iron-based bulk ferromagnets, for which magnetic softening (i.e., decrease of coercivity) can be achieved by decreasing the grain size below the material-specific magnetic correlation length.[65–68] Further potential strategies to modify the magnetic heating performance of iron oxide nanoparticles include doping and interfaces, as discussed below.

2.2. Defect-Rich Iron Oxide Nanoparticles Which Excel at Magnetic Hyperthermia

Structural defects, which are routinely found in iron oxide nanoparticles, include vacancies, twinning defects,[69] grain boundaries, and interfaces.[31,63,69–73] Iron oxide nanoparticles synthesized by thermal decomposition method tend to have defected structure and interfaces that can lead to anomalous magnetic properties.[74,75] **Figure 2**e–h shows exemplarily 23 nm iron oxide nanocubes synthesized by thermal decomposition of iron oleate[37,74] Combining high-angle annular dark field scanning transmission electron microscopy (HAADF-STEM), X-ray diffraction (XRD), and electron energy loss spectroscopy

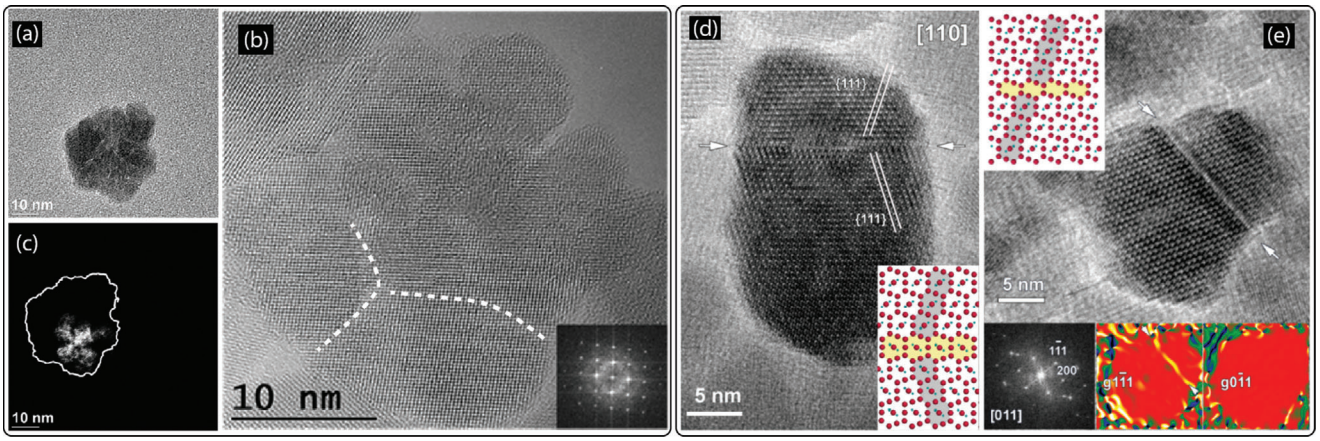

Figure 3. Grain boundaries and twinning defects in iron oxide nanoparticles. a) Typical TEM micrograph of an individual nanoflower-shaped iron oxide nanoparticle synthesized via polyol process. b) HRTEM micrograph of a single flower-like nanoparticle, so-called nanoflower. The dashed lines indicate grain boundaries between domains. c) Dark-field TEM micrograph of an individual particle showing that domains sharing the same crystallographic orientation varies between 5 to 15 nm in size. While each domain is well coherent, domains are oriented differently with respect to each other. d) HRTEM micrograph of an iron oxide nanoparticle synthesized via hydrothermal method. The nanoparticle shows a twinning defect along (111) plane, as indicated by white arrows. Inset shows atom arrangement along the twinning plane that is highlighted in yellow. The flipping of the atomic arrangement of Fe_3O_4 around the (111) twinning plane is apparent. e) HRTEM micrograph of a so-called dimer iron oxide nanoparticle synthesized via hydrothermal method, showing a grain boundary defect along (111) crystalline plane. Inset at the top shows atoms arrangement along the grain boundary that is colored in yellow. Inset at the bottom-left presents Fourier-transform diffraction pattern and insets at the bottom-right show GPA maps of $g1\bar{1}1$ and $g0\bar{1}1$ planes. The left side GPA map indicates lattice distortion along the grain boundary plane, that is, (111), as seen by a discontinuity in the color map at the grain boundary. No lattice distortion is observed along out-of-grain boundary planes, for example, (011), as shown in the right side GPA color map. a,c) Adapted with permission.[35] Copyright 2018, American Chemical Society. b) Adapted with permission.[33] Copyright 2012, American Chemical Society. d,e) Adapted with permission.[69] Copyright 2014, American Chemical Society.

(EELS), it has been observed that thermal annealing of PEGylated nanocubes at 80 °C for 48 h induces Fe^{2+} vacancies in the particle crystal structure. The Fe^{2+} vacancies together with ever remaining FeO-subdomains within the particles led to comparatively small effective *KV*. Remarkably, the thermally treated nanocubes preserved their improved intracellular magnetic hyperthermia, as evaluated by in vitro SAR measurements during interaction and uptake by IGROV-1 breast cancer cells (Figure 2k). Note that single-phase magnetite nanocubes with same size lose their heating performance nearly completely in viscous media.[76] Thus, these mildly treated nanocubes can be regarded as a prototype for improved magnetic heating by *defect-induced* magnetic softening.

Flower-shaped iron oxide nanoparticles[32,33] represent a different, prominent example for large, defect-rich iron oxide nanoparticles. As can be seen in **Figure 3**a,b,c, the nanoflowers are 20–100 nm aggregates consisting of small ≈5–15 nm maghemite crystallites.[77] The small crystallites are separated by grain boundaries, as highlighted by the dashed lines in Figure 3b. Nanoflowers belong to a special class of magnetic nanoparticles, namely multicore particles,[48,78] which are essentially stable clusters of small iron oxide crystallites or grains.[79,80] The development of multicore particles was promoted by a superior performance of such clusters in comparison to their individual building blocks for a variety of biomedical applications,[81,82] including hyperthermia.[81] The unique feature of nanoflowers is their dense structure. Due to exchange interactions between the small crystallites (Figure 3b, dashed lines), the atomic moments within the total particle volume are preferentially magnetized along the same direction, leading to large effective moments at low fields. Therefore, nanoflowers can be regarded as individual particles but which possess a nanocrystalline substructure. As a result of the grain boundaries, however, the nanoflowers exhibit a significant internal spin disorder,[35] something which is also observed for nanocrystalline bulk samples of Ni.[83] This spin disorder results in nearly vanishing coercivities,[84] analogous to nanocrystalline bulk ferromagnets.[65–68] Consequently, such nanoflowers and similar dense iron oxide nanoparticle aggregates, excel at magnetic hyperthermia at low field amplitudes.[32–36,84–86] We attribute the increased heating to the magnetic softening, which results in increased $\chi''(\omega)$ at low-field amplitudes similar to single-core thermally treated nanocubes discussed before (Figure 2).

An additional remarkable feature of nanoflowers is that their already outstanding heating performance can even be further increased with magnetic interactions at the mesoscale.[34] This can be related to a parallel alignment between neighboring particle moments within dense aggregates.[87] This behavior is in contrast to conventional interacting iron oxide nanoparticle systems (i.e., dense powder samples of single-core particles), in which an antiparallel alignment of neighboring particle moments has been observed,[88,89] culminating in reduced susceptibility and decreased heating.[90]

As highlighted above, there are multiple iron oxide nanoparticle systems in which structural defects contribute positively to enhancing the performance for biomedical applications that are based on the Néel relaxation mechanism such as magnetic hyperthermia and MPI. In the following, we will review the interrelation of structural and spin disorder in magnetic nanoparticles that is expected to be decisive for their functionality. We will then expand our discussion on the current status regarding defect-engineering in iron oxide nanoparticles, to postulate new

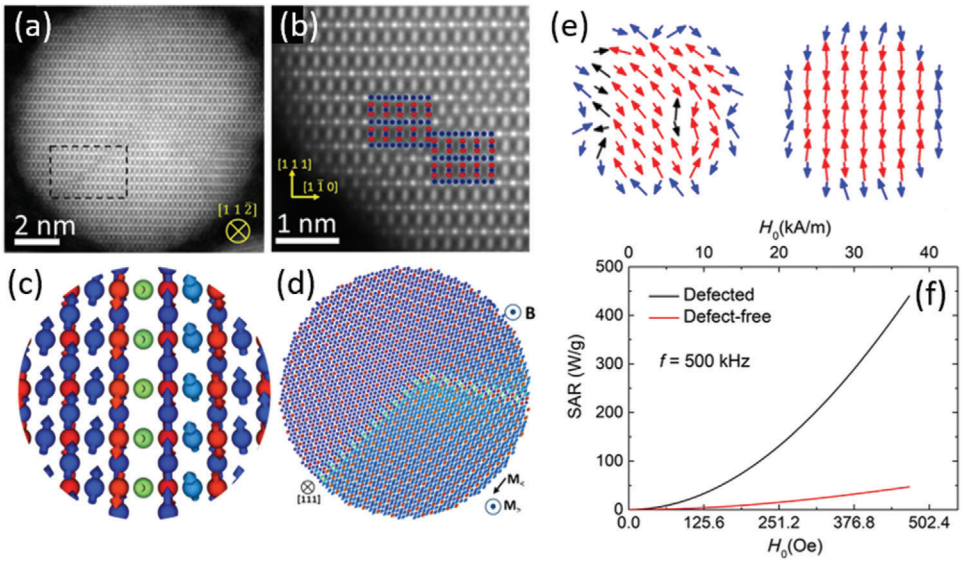

Figure 4. From structural defects in nanoparticles to spin disorder and enhanced magnetic heating performance. a) Anti-phase boundary in a representative iron oxide nanoparticle, atomically resolved using HAADF STEM. b) Magnification of the dashed area indicated in (a). c,d) Atomistic spin calculations illustrate the spin misalignment near antiphase boundaries in model nanoparticles. e) Monte Carlo simulation of the spin ensemble in a defected (left) and a defect-free nanocrystal (right) near field reversal after saturation. f) Specific absorption rate calculated for defected and defect-free nanoparticles. a–d) Reproduced with permission.[71] Copyright 2017, Springer Nature. e,f) Reproduced with permission.[63] Copyright 2019, American Physical Society.

pathways for exploiting structural defects in favor of particle performance in biomedical applications.

3. Defect-Induced Spin Disorder in Iron Oxide Nanoparticles

In the previous section, we introduced several examples of structurally disordered iron oxide nanoparticles that exhibit greatly enhanced performance in biomedical applications, in particular magnetic hyperthermia. Structural deviations from homogeneity can cause atomistic disorder of the magnetic spin ensemble and thus significantly alter the particle properties. In addition, nanoscale surface effects naturally play a decisive role in nanoparticles due to large surface-to-volume-ratio which can also cause localized spin disorder. The spin disorder in magnetic nanoparticles thus needs to be addressed to fully understand the interrelation between defects and disorder and the technological performance of magnetic nanoparticles. Despite recent advances in both microscopy and scattering approaches, resolving the magnetization configuration at the nanoscale,[91] including the complex spin configuration within magnetic nanoparticles, remains a key challenge in nanomagnetism.

Whereas long-range order is routinely characterized using diffraction techniques assuming periodic boundary conditions, the local, short range nature of disorder effects requires combination of a variety of techniques on different length scales as well as a model adapted to the length scale that is probed. Structural defects within individual magnetic nanoparticles are typically investigated with high-resolution electron microscopy techniques (**Figure 4**a,b),[71] whereas advanced scattering techniques such as synchrotron X-ray total scattering coupled with pair distribution function (PDF) analysis[26,63] or X-ray circular dichroism (XMCD)[92] provide ensemble-averaged information on the stoichiometry and crystal structure and the element-specific spin and orbital moments, respectively.

Methodology toward spin disorder includes magnetometry,[93] Mössbauer[94] and Raman spectroscopy,[95] nuclear magnetic resonance (NMR),[96] Lorentz transmission electron microscopy (LTEM),[97] high-resolution electron loss spectroscopy (HR-EELS),[70] and magnetic neutron diffraction[98] and small-angle neutron scattering (SANS).[99] Each of these techniques can provide unique information but only at specific length scales. Therefore, often combinations of various techniques are needed to acquire a self-consistent picture.

3.1. Spin Disorder at Different Scales

The existence of spin disorder in nanoparticles is typically concluded from low magnetization as compared to the bulk materials,[93,100] accompanied by nonsaturating magnetic behavior[101] and exchange biasing,[102] all observed using macroscopic magnetization measurements. Furthermore, temperature- and frequency-dependent AC susceptibility measurements were used in several studies to reveal the spin dynamics of uncorrelated surface spins and the resulting spin-glass-like freezing at low temperatures.[103–105] Microscopic information on spin disorder, that is, atomic spins deviating from the collinear order of the material, is accessible through the hyperfine structure of in-field Mössbauer spectroscopy.[106] In combination with macroscopic magnetization and X-ray diffraction, the generally assumed nanoscale model of a collinear macrospin surrounded by surface-near spin disorder (Figure 1c) is typically applied.[107–110] Surface spin disorder is understood as a result of

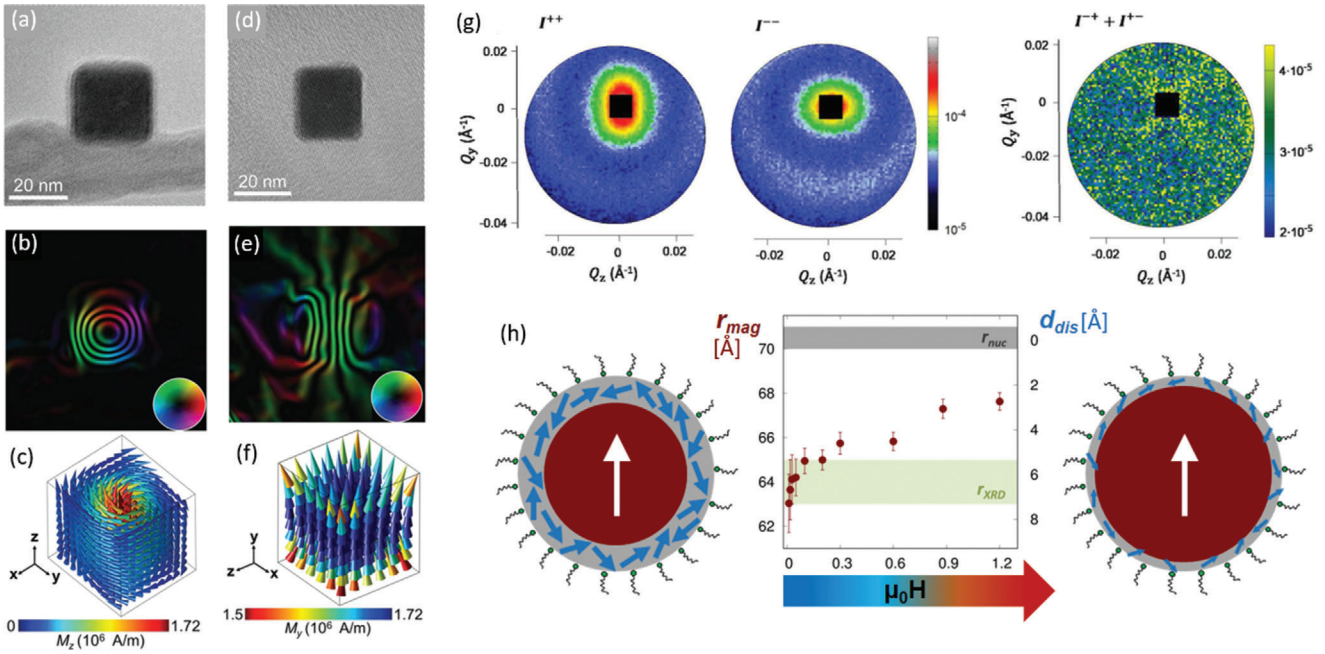

Figure 5. Nanoscale magnetization in magnetic nanoparticles. a–f) Magnetic electron holography of vortex (a–c) and single-domain (d–f) spin configurations in Fe nanoparticles. a,d) Experimental hologram; b,e) magnetic induction flux line maps derived from the experimental phase image (inset: color wheel indicating the direction of the magnetic induction). c,f) Micromagnetic simulation of the 3D magnetization of a 29.5^3 nm^3 and a $24 \times 26 \times 24$ nm^3 Fe nanocube in equilibrium state, indicating the vortex and single-domain configurations, respectively. g) Magnetic SANS data by cobalt ferrite nanoparticles in applied magnetic field of 1.2 T. The non-spin-flip channels I^{++} and I^{--} give access to the structural morphology and collinear magnetization distribution (i.e., the magnetization component parallel to the applied field). The spin-flip channels I^{+-} and I^{-+} provide a combination of collinear magnetization and spin misalignment. h) Field dependence of the thickness d_{dis} of the surface-near spin disorder shell in ferrite nanoparticles. In increasing applied magnetic field, the size of the collinearly magnetized nanoparticle core r_{mag} overcomes the structurally coherent grain size r_{XRD}, leaving a reduced shell of spin disorder. a–f) Adapted with permission.[112] Copyright 2015, American Chemical Society. g,h) Adapted with permission.[117] Copyright 2020, American Physical Society.

broken exchange bonds and low symmetry near the particle surface. Moreover, the correlation of structural and spin disorder is widely accepted. Within the macrospin model, spin disorder is hence mostly attributed to surface effects based on a particle size dependence of macroscopic magnetization properties, or based on a structurally coherent magnetic grain size smaller than the particle itself, as accessible through neutron diffraction.[98] To unambiguously confirm the location of spin disorder near the particle surface, spatially sensitive techniques are required with subnanometer resolution.

LTEM provides information on the stray field magnetization with spatial resolution of a few nanometers and can hence be applied to individual particles with sizes as small as a few nanometers.[97] Electron holography provides higher spatial resolution and is sensitive to the entire nanoparticle spin configuration and has been applied to the magnetic interparticle coupling in arrangements of nanoparticles.[111] On the individual nanoparticle level, high-resolution magnetic maps of individual Fe nanocubes have been generated to reveal the size-induced transition between vortex (**Figure 5**a–c) and single-domain states (Figure 5d–f) within the nanoparticles.[112] Whereas defect-free nanoparticles have been targeted for such proof-of-principle studies, application of electron holography techniques to the defect-induced spin structure in magnetic nanoparticles will be a challenging and highly interesting endeavor. HR-EELS is both spatially and element-sensitive and has elucidated the site-dependent surface spin canting in cobalt ferrite nanoparticles, revealing surface spin canting for the cobalt sites, but not for the iron sites.[70]

Magnetic SANS is sensitive to nanoscale magnetic fluctuations with sub-nanometer spatial resolution, giving access to the spatially resolved magnetization distribution as well as directionally resolved magnetization correlations in magnetic nanoparticles.[99] Through the spatial sensitivity with length scales of 0.1–500 nm, surface spin disorder[113] and correlated surface spin canting[114,115] become accessible. Using magnetic SANS, a significant reduction of surface spin disorder was found upon cooling to low temperatures of 10 K.[116] More recently, a strong field-dependence of surface spin disorder was revealed, expressed by a gradual polarization of initially disordered surface spins even beyond the structurally coherent grain size (Figure 5h).[117] The field dependence of the spatial distribution of surface spin disorder ultimately gives access to the spatially resolved disorder energy toward the particle surface.[117]

Nanoscale surface effects have recently been exploited toward hollow nanoparticles. The high magnetic disorder in these particle shells was attributed to two antiferromagnetically coupled noncollinear structures close to speromagnets based on a broad distribution of hyperfine fields as determined from Mössbauer spectroscopy.[118]

3.2. Spin Disorder—Correlated or Not?

Spin disorder may in a first approach be understood as the deviation of individual atomic spins from a long-range ordered, often times collinear order. An important distinction is whether spin disorder is entirely random, that is, without any correlation between adjacent spins, or correlated, that is, exhibiting short-range correlations, a scenario we will refer to as spin canting as opposed to random spin disorder in nanoparticles. Depending on surface and magnetocrystalline anisotropies, different types of spin canting toward the particle surface have been suggested by theory, including so-called artichoke, throttled, and hedgehog spin structures.[119] However, experimental evidence for such structures is scarce. The size-dependent spin structures in manganese–zinc ferrite nanoparticles were studied using unpolarized SANS in combination with micromagnetic simulations, revealing increased magnetic inhomogeneity with particle size and correlated, non-collinear spin states occurring for particle sizes beyond 20 nm.[120]

Correlated spin canting has been reported for assemblies of smaller, ≈10 nm nanoparticles,[114,115] without directly discriminating one of the suggested spin structures. In contrast, noninteracting ferrite nanoparticles of similar size reveal random surface spin disorder without a traceable coherent transversal magnetization component.[117] In consequence, a strong impact of interparticle interactions on spin disorder and spin canting is evident and needs to be considered for applications of spin disorder toward magnetic heating.

3.3. Spin Disorder in the Particle Interior

Whereas the commonly accepted macrospin model including surface spin disorder is sufficient to explain a large fraction of macroscopic phenomena, the potential existence of atomistic spin disorder in the particle interior (Figure 1d) is often disregarded. The spin disorder distribution within magnetic nanoparticles is only accessible using techniques that are both quantitative and spatially sensitive. Indeed, polarized SANS has revealed significant contributions of spin disorder even in the particle interior,[121] expressed as a reduced local magnetization in the particle core.[113,116,117] In several reports, the spin disorder in the particle interior has even been found to dominate surface spin disorder.[113,122] Such a reduced magnetization has been attributed to canting of Fe moments in both tetrahedral and octahedral sites, revealed by a combination of NMR and Mössbauer spectroscopies, and related to reversed moments and frustrated topology.[96]

A clear particle size dependence of spin disorder in iron oxide nanoparticles has been established using Mössbauer spectroscopy, revealing enhanced spin canting in an intermediate particle size of 8–12 nm.[31] Combination of magnetic SANS with nuclear resonant X-ray scattering has further revealed a clear atomic site dependence of the spin misalignment.[122] The significant amount of spin disorder found in the nanoparticle interior underlines that disorder and defects on the atomic scale are highly relevant to understand and control the nanoscale and macroscopic magnetic properties in nanoparticles.

Indeed, structural distortions changing the local coordination geometry in the vicinity of defects have a direct influence on interatomic exchange and hence spin disorder.[123] For ferrite nanoparticles, strong variations of the degree of spinel inversion are commonly observed.[124–128] The synthesis technique has been reported to substantially influence the ferrite nanoparticle magnetization and, hence the spin disorder,[71] through structural defects such as antiphase boundaries resulting from topotactic oxidation from FeO to maghemite (see Figures 2a–d and 4a–d).[74] Antiphase boundaries have further been found to induce local ferromagnetic coupling and enhance the magnetic properties of magnetic nanoparticles.[129] Local disorder, resulted by atomic-scale defects, that triggers a correlated structural distortion has recently been discovered in core–shell Fe_xO-$Fe_{3-\delta}O_4$ nanocrystals by analysis of the atomic pair distribution function and correlated with atomistic spin disorder and enhanced magnetic heating efficiencies (Figure 4e,f).[63] Despite only few studies published to date, we expect more studies to appear on technological benefits of defect-induced magnetic lattice distortions in magnetic nanoparticles in the near future. All these findings illustrate that for a comprehensive understanding of the macroscopic performance of magnetic nanoparticles, it is indispensable to consider both structural and spin disorder on a variety of length scales (Figure 1), including the nanoscale magnetization distribution, but also the atomistic scale defect-induced disorder in magnetic nanoparticles.

Having established the potential of structural and magnetic disorder for improved magnetic hyperthermia performance, we next highlight current synthetic approaches on how to deliberately engineer defects and disorder in iron oxide nanoparticles.

4. Defect-Engineering in Iron Oxide Nanoparticles

4.1. Colloidal Synthesis: A Journey toward Disordered Iron Oxide Nanoparticles

The quest to synthesize defect-free and single-crystalline magnetic nanoparticles dates back to almost 20 years ago when the first colloidal thermal decomposition syntheses emerged. Varieties of iron precursors including organometallic $Fe(C_6H_5N(O)NO)_3$,[130] metal organic $Fe(CO)_5$,[131] $Fe(acac)_3$,[132] metal hydroxide FeO(OH),[133] and iron salts such as Fe(II) acetate,[134] have been used for synthesis of iron oxide nanoparticles. Large-scale size and shape-control synthesis of iron oxide nanoparticles have been realized after developing $Fe(oleate)_3$ by Hyeon et al.[135] Despite differing in solvent, capping ligands, and growth temperature, in these non-hydrolytic syntheses, nanoparticles are mostly a product of kinetically driven processes, for example, through adsorption/desorption of capping ligands on certain crystalline facets.[136] Thanks to the kinetic pathways, the formation of uniformly sized and shaped iron oxide nanoparticles often takes no longer than an hour in these methods.[137] The chemical nature of the iron precursor used for the synthesis has a substantial influence on the type, distribution, and abundance of defects in nanoparticles. Whereas $Fe(acac)_3$ often results in particles with nearly absent surface spin canting,[138,139] detailed characterization studies have revealed that $Fe(CO)_5$, $Fe(oleate)_3$, and Fe(II) acetate lead to FeO-Fe_3O_4/Fe_2O_3 and Fe-Fe_3O_4[140] core–shell iron oxide nanoparticles with degraded magnetization

and structural disorders.[134,141–144] Several groups have developed twists in the decomposition chemistry[145] and modified the synthesis involving protective gas[146,147] to eliminate the FeO phase, showing a weak paramagnetic behavior at hyperthermia relevant temperatures, and obtain single-phase Fe_3O_4 nanoparticles. Further approaches reduce surface spin disorder in superparamagnetic ferrite magnetic nanoparticles by changing the nature of alkaline capping agents.[148]

Despite the progress, we know from solid state chemistry and materials science that defect-free crystals are the product of thermodynamically driven processes, forming at much higher temperatures and longer reaction times than that of colloidal syntheses (i.e., 220–340 °C, <1h). Moreover, recent magnetic hyperthermia studies have strikingly shown that defect-free and highly crystalline single-core iron oxide nanoparticles lose nearly entirely their hyperthermia efficacy in highly viscous media,[76] in vitro,[49] and intracellularly.[37,51] Di Corato et al. have systematically shown this phenomenon in vitro for multicore and cubic-shape single-core iron oxide nanoparticles.[49]

The tendency to compare physicochemical properties of synthetic iron oxide nanoparticles such as saturation magnetization and magnetic anisotropy with the bulk-like properties has thus far distracted us from exploring defects and disorders in favor of biomedical applications. In the following, we will briefly discuss current synthetic approaches for defect- and disorder-engineering in single-phase and interfaces in core-shell iron oxide nanoparticles with particular focus on their impact on magnetic hyperthermia.

4.2. Defects and Discontinuities Induced by Growth Pathways

Capping ligands are an indispensable part of thermal decomposition syntheses, as they control size and morphology of nanocrystals by influencing the reaction kinetics. Playing with the binding nature and strength between capping agents and nanocrystals has always been an effective strategy to control particle shape and size.[149,150] Recently, capping ligands were exploited to change the internal structure of iron oxide nanoparticles. A prime example is iron oxide nanoflowers (Figure 3a–c), wherein short length polyols such as diethylene glycol allows packing small crystallites into dense disordered structures, being separated by grain boundary defect (dashed lines in Figure 3b).[77,151] The effect of competition between short and long ligands on the particle structure has recently been shown in zinc ferrite nanoparticles. Increasing the ratio of acetylacetone to oleic acid ligands results in assembly of small magnetic zinc ferrite subdomains into 100 nm cubic-shape particles, due to less bulkiness and higher mobility of acetylacetone ligands as compared to oleic acid.[152]

Hydrothermally synthesized iron oxide nanoparticles showed to possess twinning and stacking fault defects (Figure 3d,e).[69] Formation of twinning defects and stacking faults along (111) crystalline planes was attributed to the oriented-attachment crystal growth mechanism. A growth mechanism similar to the nanoflowers was proposed for these defected iron oxide nanoparticles. The fusion of initial Fe_3O_4 crystallites, that is promoted by desorption of capping ligands, into a single particle accounts for twinning and stacking fault defects. Interestingly, none of these defects were observed when a similar synthesis mixture was treated by co-precipitation synthesis method. It was therefore discussed that an intensive activity and mobility of the capping ligands on crystallites, given to the synthesis reaction by high temperature hydrothermal reaction conditions, is required to form defect-rich iron oxide nanoparticles. Remarkably, it was demonstrated that iron oxide nanoparticles with stacking fault internal defects have a higher M_s and SAR than defect-free iron oxide nanoparticles.[69]

4.3. Defects and Vacancies Induced by Oxidation

Most iron oxide nanoparticles synthesized via thermal decomposition syntheses have to some extent defects, disorders, and sub-domains. Iron oxide nanoparticles synthesized via the thermal decomposition of $Fe(oleate)_3$ and $Fe(CO)_5$ are among the most heavily characterized nanoparticle systems due to the synthesis robustness and particle size uniformity.[26,144,153] However, these two precursors predominantly lead to FeO-Fe_3O_4 core–shell morphologies instead of phase-pure Fe_3O_4 composition. Such a core-shell formation, having the often non-stoichiometric Fe_xO ($x \approx 0.95$) phase,[37,154] leads to a large dispersion of magnetic properties that requires a very detailed systematic characterization.[154] Studies on post synthesis thermal treatment of these iron oxide nanoparticles toward single-phase iron oxide have led to new insights into oxidation-induced defects. It has been shown that the nucleation and growth of Fe_3O_4 on the FeO phase (i.e., the topotaxial oxidation from FeO to magnetite and maghemite) lead to formation of antiphase boundary (APB) defects at the interface between growing magnetite domains. Interestingly, APBs remained after four hours of thermal treatment at 150 °C (Figure 2a–d).[74] The oxidation of core–shell iron oxide nanoparticles, synthesized by decomposition of $Fe(CO)_5$, via mild cyclic magnetic stimulations has also resulted in the APBs.[155]

A step toward exploiting structural defects for biomedical applications was taken by mild thermal treatment of FeO-Fe_3O_4 nanoparticles after being capped with catechol-terminated functional poly(ethylene glycol) polymers. A 48 h thermal treatment at 80 °C induced Fe^{2+} vacancies in the Fe_3O_4 phase of core–shell iron oxide nanoparticles, which result in the magnetic softening and thus the domination of the Néel relaxation. As discussed in the previous section, such a magnetic softening can lead to improved magnetic hyperthermia performance of 23 nm cubic-shape particles compared to single-phase counterparts (Figure 2e–k).[37] It is worth mentioning that in case of small nanoparticles a defect-induced magnetic hardening may be necessary to tailor the magnetic heating performance.[63]

4.4. Structural Defects Associated with Interfaces and Doping

Interfaces are additional promising sources of breaking composition continuity and inducing atomic scale exchange interactions in magnetic nanoparticles. The magnetic anisotropy can be tuned by magnetic coupling in bi-magnetic hard-soft and soft-hard core-shell magnetic nanoparticles such as $CoFe_2O_4$-$MnFe_2O_4$[156] and Fe_3O_4-$CoFe_2O_4$.[157] More in depth insight into these nanosystems can be found in the review by López-Ortega

et al.[158] The effect of thickness and composition of the shell on the magnetization of bi-magnetic exchanged bias nanosystems has already been discussed more than a decade ago.[159] However, the implication of bi-magnetic nanoparticles in in vivo magnetic hyperthermia was realized some years later. A systematic study on the effect of core size, particle shape, and shell thickness has revealed an enhanced magnetic-to-heat energy transformation in core–shell nanoparticles.[160] It was recently shown that forming an ultrathin shell of soft magnets (e.g., Fe_3O_4 and $MnFe_2O_4$) on $CoFe_2O_4$ nanoparticles leads to increased magnetic anisotropy.[161,162] The shell thickness turned to be critical to observe a so-called enhanced spin canting phenomenon. Inserting a paramagnetic FeO interlayer spacer between Fe core and iron oxide shell in layered iron oxide nanoparticles led to magnetostatic interactions between the core and the shell and enhanced magnetic hyperthermia performance.[73] Recently, trimagnetic Fe_3O_4-CoO-Fe_3O_4 core–shell–shell nanoparticles have been developed via seed-mediated thermal decomposition synthesis. Hard–soft exchange couplings at Fe_3O_4-Co doped ferrite and Co-doped ferrite-Fe_3O_4 interfaces largely influenced the superparamagnetic blocking temperature and magnetization hysteresis loops.[163] Despite being a promising approach, one has to bear in mind that synthesis of multi layered nanoparticles is much more challenging than those iron oxide nanoparticles formed via one-pot reactions.

Theoretical studies have contributed substantially to our understanding of magnetization mechanisms in such multilayered particle systems. The Monte Carlo approach has been exploited to reconstruct the magnetic spin configuration in Fe-Fe_3O_4 core–shell nanoparticles with different shapes[164] and has proven antiferromagnetic coupling in soft-hard Fe_3O_4-Mn_3O_4 core–shell nanoparticles, in accordance with the experimental results.[165]

Breaking the cation ordering by doping magnetic[166] and nonmagnetic ions into the iron oxide crystal structure has emerged as a strong tool to tune magnetic properties in the past years.[138,167] For spinel ferrite nanoparticles, the cation distribution between A and B sites is decisive for the macroscopic magnetization, and strong variations of the inversion degree have been observed as nanoparticles often represent a non-equilibrium cation distribution.[124–126] Zinc and manganese are the most commonly substituted cations into iron oxide nanoparticles.[168] Despite being nonmagnetic, Zn^{2+} replaces Fe^{3+} in tetrahedral crystalline sites and thus reduces antiferromagnetic couplings between Fe^{3+} in tetrahedral and octahedral sites. Depending on the ionic size and concentration of the substituting cation, lattice strain was induced in cobalt ferrite nanoparticles.[169,170] Such approach appears promising to tailor the lattice strain and in result control the magnetization of iron oxide nanoparticles.

5. Conclusions and Perspectives

The strong research interest on iron oxide nanoparticles is particularly driven by their unique potential for a wide range of biomedical applications. To optimize their magnetic properties, historically, the usual strategy has been to strive for the synthesis of defect-free single crystalline nanoparticles. The particle characteristics have been then primarily varied by their morphological features such as size and shape. In this progress report we have compiled recent findings indicating an alternative approach for improving magnetic particle properties. Inspired by other research fields such as semiconductors and perovskite solar cells, we here attempt to redirect the attention of the magnetic nanoparticle community toward exploiting defect-engineering in iron oxide nanoparticles to enhance and adapt particle magnetic properties for in vivo magnetic hyperthermia. Approaches to the design of defected structures have very recently been summarized for bulk crystalline materials.[171]

Recent experimental and computational studies emphasize a clear benefit of structural defects and associated magnetic spin disorder in various biomedical applications. Defect-rich iron oxide nanoparticles appear particularly promising candidates for intracellular magnetic hyperthermia and magnetic-heating-triggered drug delivery, wherein transducing heat based on the Néel magnetic relaxation mechanism is crucial. Sharing similar nanomagnetism principles to magnetic hyperthermia,[172] MPI, an emerging molecular imaging modality, will largely benefit from defect-engineering in iron oxide nanoparticles. The research on developing iron oxide based tracers for MPI is growing rapidly owing to outstanding features of MPI compared to MRI such as high sensitivity, deep tissue imaging, and capability of live imaging.[173] It is well known that the MPI imaging technique works based on the Néel relaxation mechanism. Therefore, iron oxide nanoparticles with the characteristics highlighted here for large and defect-rich iron oxide nanoparticles, that is, large magnetic susceptibility and low magnetic anisotropy, are well suited for MPI. This correlation was verified by several studies which conclude that nanoflowers are excellent candidates for MPI.[38,39]

We have here summarized studies on synthesis of defect-rich iron oxide nanoparticles, yet our focus is on those studies in which defects and disorder have been mainly included deliberately. We have highlighted few one-pot synthesis reactions and post synthesis thermal treatments in organic solvents and aqueous media that promote structural defects and compositional discontinuities in iron oxide nanoparticles. Anti-phase boundaries, stacking faults, grain boundaries, and twinning defects have been induced in iron oxide nanoparticles.

Looking into the correlation between structural and magnetic lattice, we have realized that one important aspect that is often overlooked is the different characteristics of spin disorder on nanoscale and atomistic length scales. The magnetic structure of iron oxide nanoparticles is directly determined by their structural features, implying that structural defects lead to disordered magnetic lattice and eventual modification of the magnetic properties. Despite the progress in atomistic analyses, the precise characterization of spin disorder within the particles remains one of the key challenges in nanomagnetism. However, it is crucial to distinguish between surface-induced nanoscale spin disorder and atomistic, structurally induced intraparticle spin disorder when assessing macroscopic magnetic properties and hence technological performance of magnetic nanoparticles.

Admittedly, the programmed defect inclusion in iron oxide nanoparticles is yet in its infant stage, when compared to other fields such as semiconductor technology. However, the number of research articles on revealing and harnessing positive contribution of defects is rapidly growing. In the following, we add our perspectives and ideas on how to systematically engineer defects into the crystal structure of iron oxide nanoparticles.

One of the potential approaches to synthesize iron oxide nanoparticles with grain boundaries like nanoflowers discussed here is to use a combination of short and long capping ligands with different binding affinities to iron. A combination of short phosphonate-based and oleic acid ligands in thermal decomposition synthesis could lead to the formation of iron oxide nanoparticles with grain boundaries via a competitive ligand binding to different positions on particles. The nature of binding between capping ligands and particles is yet largely unknown and thus more elucidations in this regard will facilitate designing disorder in iron oxide nanoparticles.

We envision a great opportunity in combining crystalline disorder and in vivo clearance of magnetic nanoparticles in developing defect-rich nanoheaters and MPI tracers. We believe a novel synthetic approach could be to fabricate nanoparticle organic frameworks (NOFs), wherein nanoparticles are assembled together with responsive molecules such as peptides and short oligonucleotides. Controlling size and polydispersity of these assemblies, NOFs might behave similarly to nanoflowers and excel at intracellular magnetic hyperthermia. The unique feature of NOFs, non-existent in nanoflowers, is the capability of being dissociated to small building blocks that can be easily cleared from the body. NOFs will be particularly promising for magnetic monitoring of drug release, wherein a frequent injection of nanocarriers, for example, once a week and thus a rapid clearance of previously administrated nanocarriers is needed to not interfere with newly coming ones in terms of magnetic signal.

A further strategy is doping-induced-defects by replacing iron with magnetic and nonmagnetic cations such as Cu, Co, Zn, or Gd.[174,175] Doping in iron oxide nanoparticles has traditionally been mainly used to reduce compensating magnetic couplings and improve magnetization, as in the case of Zn^{2+} in iron oxide nanoparticles. We envision the opportunity of inducing other defects and thus tailoring magnetic anisotropy of nanoparticles by defect-induced distortion of the magnetic lattice. Doping appeared as a powerful tool to improve electrical properties of semiconductors[6] and modify photonic properties of quantum dots.[176] Studies on doping-induced-defects in iron oxide nanoparticles seem to lack behind other technological fields, which call for employing a combination of atomistic analyses to unveil defects and their impacts on magnetic properties in near future to come.

To sum up, we advocate our review will stimulate further research and development on novel synthetic routes for defect-engineering as well as selecting appropriate characterization methods depending on the type of defect in magnetic nanoparticles. Eliminating the negative connotation associated with defects and disorder in magnetic nanoparticles, our report will set the scene for embracing the structural and magnetic lattice disorders in magnetic nanoparticles to further advance in vivo biomedical applications.

Acknowledgements

A.L., S.D., and P.B. contributed equally to this work. S.D. acknowledges financial support from the German Research Foundation (DFG Grant DI 1788/2-1). A.L. acknowledges the Alexander von Humboldt Foundation for postdoctoral research fellowship. P.B. acknowledges financial support from the Fonds National de la Recherche Luxembourg (CORE SANS4NCC grant, C17/MS/11661571).

Conflict of Interest

The authors declare no conflict of interest.

Keywords

defect-engineering, design-by-disorder, iron oxide nanoparticles, magnetic hyperthermia, magnetic spin disorder

Received: July 16, 2020
Revised: October 30, 2020
Published online: February 15, 2021

[1] S. K. Estreicher, *Mater. Today* **2003**, *6*, 26.
[2] G. I. Márk, Z. Vértesy, K. Kertész, Z. Bálint, L. P. Biró, *Phys. Rev. E* **2009**, *80*, 051903.
[3] P. Vukusic, B. Hallam, J. Noyes, *Science* **2007**, *315*, 348.
[4] E. Lurie-Luke, *Biotechnol. Adv.* **2014**, *32*, 1494.
[5] D. S. Wiersma, *Nat. Photonics* **2013**, *7*, 188.
[6] H. J. Queisser, E. E. Haller, *Science* **1998**, *281*, 945.
[7] W. J. Yin, T. Shi, Y. Yan, *Appl. Phys. Lett.* **2014**, *104*, 063903.
[8] X. Li, K. Lu, *Nat. Mater.* **2017**, *16*, 700.
[9] T. Rojac, A. Bencan, G. Drazic, N. Sakamoto, H. Ursic, B. Jancar, G. Tavcar, M. Makarovic, J. Walker, B. Malic, D. Damjanovic, *Nat. Mater.* **2017**, *16*, 322.
[10] T. C. Shyu, P. F. Damasceno, P. M. Dodd, A. Lamoureux, L. Xu, M. Shlian, M. Shtein, S. C. Glotzer, N. A. Kotov, *Nat. Mater.* **2015**, *14*, 785.
[11] A. V. Krasheninnikov, F. J. Banhart, *Nat. Mater.* **2007**, *6*, 723.
[12] Y. Wei, J. Wu, H. Yin, X. Shi, R. Yang, M. Dresselhaus, *Nat. Mater.* **2012**, *11*, 759.
[13] A. B. Cairns, A. L. Goodwin, *Chem. Soc. Rev.* **2013**, *42*, 4881.
[14] D. A. Keen, A. L. Goodwin, *Nature* **2015**, *521*, 303.
[15] A. R. Overy, A. B. Cairns, M. J. Cliffe, A. Simonov, M. G. Tucker, A. L. Goodwin, *Nat. Commun.* **2016**, *7*, 10445.
[16] A. Simonov, T. De Baerdemaeker, H. L. B. Boström, M. L. Ríos Gómez, H. J. Gray, D. Chernyshov, A. Bosak, H. B. Bürgi, A. L. Goodwin, *Nature* **2020**, *578*, 256.
[17] Y. Zhang, G. M. Stocks, K. Jin, C. Lu, H. Bei, B. C. Sales, L. Wang, L. K. Béland, R. E. Stoller, G. D. Samolyuk, M. Caro, A. Caro, W. J. Weber, *Nat. Commun.* **2015**, *6*, 8736.
[18] M. S. Mrudul, N. Tancogne-Dejean, A. Rubio, G. Dixit, *npj Comput. Mater.* **2020**, *6*, 10.
[19] R. Friedberg, D. I. Paul, *Phys. Rev. Lett.* **1975**, *34*, 1234.
[20] A. Michels, D. Mettus, I. Titov, A. Malyeyev, M. Bersweiler, P. Bender, I. Peral, R. Birringer, Y. Quan, P. Hautle, J. Kohlbrecher, D. Honecker, J. R. Fernández, L. F. Barquín, K. L. Metlov, *Phys. Rev. B* **2019**, *99*, 014416.
[21] S. Mühlbauer, B. Binz, F. Jonietz, C. Pfleiderer, A. Rosch, A. Neubauer, R. Georgii, P. Böni, *Science* **2009**, *323*, 915.
[22] D. Sander, S. O. Valenzuela, D. Makarov, C. H. Marrows, E. E. Fullerton, P. Fischer, J. McCord, P. Vavassori, S. Mangin, P. Pirro, B. Hillebrands, A. D. Kent, T. Jungwirth, O. Gutfleisch, C. G. Kim, A. Berger, *J. Phys. D Appl. Phys.* **2017**, *50*, 363001.
[23] A.-H. Lu, E. L. Salabas, F. Schüth, *Angew. Chem. Int. Ed. Engl.* **2007**, *46*, 1222.
[24] Q. A. Pankhurst, J. Connolly, S. K. Jones, J. Dobson, *J. Phys. D Appl. Phys.* **2003**, *36*, R167.
[25] A. Jordan, R. Felix, *J. Magn. Magn. Mater.* **1999**, *201*, 413.
[26] R. U. Ichikawa, A. G. Roca, A. López-Ortega, M. Estrader, I. Peral, X. Turrillas, J. Nogués, *Small* **2018**, *14*, 1800804.

[27] C. H. Cunningham, T. Arai, P. C. Yang, M. V. McConnell, J. M. Pauly, S. M. Conolly, *Magn. Reson. Med.* **2005**, *53*, 999.
[28] G. Muscas, N. Yaacoub, D. Peddis, in *Novel Magnetic Nanostructures*, Elsevier, New York **2018**, pp. 127–163.
[29] M. H. Oh, M. G. Cho, D. Y. Chung, I. Park, Y. P. Kwon, C. Ophus, D. Kim, M. G. Kim, B. Jeong, X. W. Gu, J. Jo, J. M. Yoo, J. Hong, S. McMains, K. Kang, Y.-E. Sung, A. P. Alivisatos, T. Hyeon, *Nature* **2020**, *577*, 359.
[30] R. Massart, *IEEE Trans. Magn.* **1981**, *34*, 142.
[31] W. Baaziz, B. P. Pichon, S. Fleutot, Y. Liu, C. Lefevre, J. M. Greneche, M. Toumi, T. Mhiri, S. Begin-Colin, *J. Phys. Chem. C* **2014**, *118*, 3795.
[32] P. Hugounenq, M. Levy, D. Alloyeau, L. Lartigue, E. Dubois, V. Cabuil, C. Ricolleau, S. Roux, C. Wilhelm, F. Gazeau, R. Bazzi, *J. Phys. Chem. C* **2012**, *116*, 15702.
[33] L. Lartigue, P. Hugounenq, D. Alloyeau, S. P. Clarke, M. Lévy, J. C. Bacri, R. Bazzi, D. F. Brougham, C. Wilhelm, F. Gazeau, *ACS Nano* **2012**, *6*, 10935.
[34] D. Sakellari, K. Brintakis, A. Kostopoulou, E. Myrovali, K. Simeonidis, A. Lappas, M. Angelakeris, *Mater. Sci. Eng., C* **2016**, *58*, 187.
[35] P. Bender, J. Fock, C. Frandsen, M. F. Hansen, C. Balceris, F. Ludwig, O. Posth, E. Wetterskog, L. K. Bogart, P. Southern, W. Szczerba, L. Zeng, K. Witte, C. Grüttner, F. Westphal, D. Honecker, D. González-Alonso, L. Fernández Barquín, C. Johansson, *J. Phys. Chem. C* **2018**, *122*, 3068.
[36] P. Bender, J. Fock, M. F. Hansen, L. K. Bogart, P. Southern, F. Ludwig, F. Wiekhorst, W. Szczerba, L. J. Zeng, D. Heinke, N. Gehrke, M. T. F. Díaz, D. González-Alonso, J. I. Espeso, J. R. Fernández, C. Johansson, *Nanotechnology* **2018**, *29*, 425705.
[37] A. Lak, M. Cassani, B. T. Mai, N. Winckelmans, D. Cabrera, E. Sadrollahi, S. Marras, H. Remmer, S. Fiorito, L. Cremades-Jimeno, F. J. Litterst, F. Ludwig, L. Manna, F. J. Teran, S. Bals, T. Pellegrino, *Nano Lett.* **2018**, *18*, 6856.
[38] H. Kratz, A. Mohtashamdolatshahi, D. Eberbeck, O. Kosch, R. Hauptmann, F. Wiekhorst, M. Taupitz, B. Hamm, J. Schnorr, *Nanomaterials* **2019**, *9*, 1466.
[39] M. Wetegrove, K. Witte, W. Bodnar, D. E. Pfahl, A. Springer, N. Schell, F. Westphal, E. Burkel, *CrystEngComm* **2019**, *21*, 1956.
[40] E. Cazares-Cortes, S. Cabana, C. Boitard, E. Nehlig, N. Griffete, J. Fresnais, C. Wilhelm, A. Abou-Hassan, C. Ménager, *Adv. Drug Delivery Rev.* **2019**, *138*, 233.
[41] E. A. Périgo, G. Hemery, O. Sandre, D. Ortega, E. Garaio, F. Plazaola, F. J. Teran, *Appl. Phys. Rev.* **2015**, *2*, 041302.
[42] A. Bordet, L.-M. Lacroix, P.-F. Fazzini, J. Carrey, K. Soulantica, B. Chaudret, *Angew. Chem.* **2016**, *128*, 16126.
[43] C. Niether, S. Faure, A. Bordet, J. Deseure, M. Chatenet, J. Carrey, B. Chaudret, A. Rouet, *Nat. Energy* **2018**, *3*, 476.
[44] J. L. Urraca, B. Cortés-Llanos, C. Aroca, P. de la Presa, L. Pérez, M. C. Moreno-Bondi, *J. Phys. Chem. C* **2018**, *122*, 10189.
[45] K. Mahmoudi, C. G. Hadjipanayis, *Front. Chem.* **2014**, *2*, 109.
[46] L. Beola, L. Gutiérrez, V. Grazú, L. Asín, in *Nanomaterials for Magnetic and Optical Hyperthermia Applications*, Elsevier, New York **2019**, pp. 317–337.
[47] C. Blanco-Andujar, F. J. Teran, D. Ortega, in *Iron Oxide Nanoparticles for Biomedical Applications*, Elsevier, New York **2018**, pp. 197–245.
[48] J. Wells, O. Kazakova, O. Posth, U. Steinhoff, S. Petronis, L. K. Bogart, P. Southern, Q. Pankhurst, C. Johansson, *J. Phys. D Appl. Phys.* **2017**, *50*, 383003.
[49] R. Di Corato, A. Espinosa, L. Lartigue, M. Tharaud, S. Chat, T. Pellegrino, C. Ménager, F. Gazeau, C. Wilhelm, *Biomaterials* **2014**, *35*, 6400.
[50] S. Ota, T. Yamada, Y. Takemura, *J. Nanomater.* **2015**, *2015*, 836761.
[51] D. Cabrera, A. Coene, J. Leliaert, E. J. Artés-Ibáñez, L. Dupré, N. D. Telling, F. J. Teran, *ACS Nano* **2018**, *12*, 2741.
[52] D. Ortega, Q. A. Pankhurst, *Magnetic hyperthermia*, in *Nanoscience: Volume 1: Nanostructures through Chemistry* Royal Society of Chemistry, Cambridge, P. O'Brien, (Ed.) **2013**, pp. 60–88. https://doi.org/10.1039/9781849734844-00060
[53] K. Mahmoudi, A. Bouras, D. Bozec, R. Ivkov, C. Hadjipanayis, *Int. J. Hyperthermia* **2018**, *34*, 1316.
[54] C. L. Dennis, R. Ivkov, *Int. J. Hyperthermia* **2013**, *29*, 715.
[55] M. Kallumadil, M. Tada, T. Nakagawa, M. Abe, P. Southern, Q. A. Pankhurst, *J. Magn. Magn. Mater.* **2009**, *321*, 1509.
[56] R. R. Wildeboer, P. Southern, Q. A. Pankhurst, *J. Phys. D Appl. Phys* **2014**, *47*, 495003.
[57] R. E. Rosensweig, *J. Magn. Magn. Mater.* **2002**, *252*, 370.
[58] J. P. Fortin, C. Wilhelm, J. Servais, C. Ménager, J. C. Bacri, F. Gazeau, *J. Am. Chem. Soc.* **2007**, *129*, 2628.
[59] I. Andreu, A. Urtizberea, E. Natividad, *Nanoscale* **2020**, *12*, 572.
[60] J. L. Déjardin, F. Vernay, M. Respaud, H. Kachkachi, *J. Appl. Phys.* **2017**, *121*, 203903.
[61] K. Simeonidis, M. P. Morales, M. Marciello, M. Angelakeris, P. De La Presa, A. Lazaro-Carrillo, A. Tabero, A. Villanueva, O. Chubykalo-Fesenko, D. Serantes, *Sci. Rep.* **2016**, *6*, 38382.
[62] G. Shi, R. Takeda, S. B. Trisnanto, T. Yamada, S. Ota, Y. Takemura, *J. Magn. Magn. Mater.* **2019**, *473*, 148.
[63] A. Lappas, G. Antonaropoulos, K. Brintakis, M. Vasilakaki, K. N. Trohidou, V. Iannotti, G. Ausanio, A. Kostopoulou, M. Abeykoon, I. K. Robinson, E. S. Bozin, *Phys. Rev. X* **2019**, *9*, 041044.
[64] A. Muela, D. Muñoz, R. Martín-Rodríguez, I. Orue, E. Garaio, A. Abad Díaz De Cerio, J. Alonso, J. Á. García, M. L. Fdez-Gubieda, *J. Phys. Chem. C* **2016**, *120*, 24437.
[65] G. Herzer, *IEEE Trans. Magn.* **1990**, *26*, 1397.
[66] G. Herzer, *Scr. Metall. Mater.* **1995**, *33*, 1741.
[67] J. Ding, Y. Li, L. F. Chen, C. R. Deng, Y. Shi, Y. S. Chow, T. B. Gang, *J. Alloy. Compd.* **2001**, *314*, 262.
[68] Q. Zeng, I. Baker, V. McCreary, Z. Yan, *J. Magn. Magn. Mater.* **2007**, *318*, 28.
[69] Y. V. Kolen'Ko, M. Bañobre-López, C. Rodríguez-Abreu, E. Carbó-Argibay, A. Sailsman, Y. Piñeiro-Redondo, M. F. Cerqueira, D. Y. Petrovykh, K. Kovnir, O. I. Lebedev, J. Rivas, *J. Phys. Chem. C* **2014**, *118*, 8691.
[70] D. S. Negi, H. Sharona, U. Bhat, S. Palchoudhury, A. Gupta, R. Datta, *Phys. Rev. B* **2017**, *95*, 174444.
[71] Z. Nedelkoski, D. Kepaptsoglou, L. Lari, T. Wen, R. A. Booth, S. D. Oberdick, P. L. Galindo, Q. M. Ramasse, R. F. L. Evans, S. Majetich, V. K. Lazarov, *Sci. Rep.* **2017**, *7*, 45997.
[72] I. Castellanos-Rubio, I. Rodrigo, R. Munshi, O. Arriortua, J. S. Garitaonandia, A. Martinez-Amesti, F. Plazaola, I. Orue, A. Pralle, M. Insausti, *Nanoscale* **2019**, *11*, 16635.
[73] K. Simeonidis, C. Martinez-Boubeta, D. Serantes, S. Ruta, O. Chubykalo-Fesenko, R. Chantrell, J. Oró-Solé, L. Balcells, A. S. Kamzin, R. Nazipov, A. Makridis, M. Aagelakeris, *ACS Appl. Nano Mater.* **2020**, *3*, 4465.
[74] E. Wetterskog, C. W. Tai, J. Grins, L. Bergström, G. Salazar-Alvarez, *ACS Nano* **2013**, *7*, 7132.
[75] M. Testa-Anta, B. Rodríguez-González, V. Salgueiriño, *Part. Part. Syst. Charact.* **2019**, *36*, 1900283.
[76] D. Cabrera, A. Lak, T. Yoshida, M. E. Materia, D. Ortega, F. Ludwig, P. Guardia, A. Sathya, T. Pellegrino, F. J. Teran, *Nanoscale* **2017**, *9*, 5094.
[77] H. Gavilán, A. Kowalski, D. Heinke, A. Sugunan, J. Sommertune, M. Varón, L. K. Bogart, O. Posth, L. Zeng, D. González-Alonso, C. Balceris, J. Fock, E. Wetterskog, C. Frandsen, N. Gehrke, C. Grüttner, A. Fornara, F. Ludwig, S. Veintemillas-Verdaguer, C. Johansson, M. P. Morales, *Part. Part. Syst. Charact.* **2017**, *34*, 1700094.
[78] S. Dutz, *IEEE Trans. Magn.* **2016**, *52*, 0200103.

[79] A. Ditsch, P. E. Laibinis, D. I. C. Wang, T. A. Hatton, *Langmuir* **2005**, *21*, 6006.
[80] A. Kostopoulou, A. Lappas, *Nanotechnol. Rev.* **2015**, *4*, 595.
[81] J. F. Berret, N. Schonbeck, F. Gazeau, D. El Kharrat, O. Sandre, A. Vacher, M. Airiau, *J. Am. Chem. Soc.* **2006**, *128*, 1755.
[82] L. L. Ma, M. D. Feldman, J. M. Tam, A. S. Paranjape, K. K. Cheruku, T. A. Larson, J. O. Tam, D. R. Ingram, V. Paramita, J. W. Villard, J. T. Jenkins, T. Wang, G. D. Clarke, R. Asmis, K. Sokolov, B. Chandrasekar, T. E. Milner, K. P. Johnston, *ACS Nano* **2009**, *3*, 2686.
[83] A. Michels, R. N. Viswanath, J. G. Barker, R. Birringer, J. Weissmüller, *Phys. Rev. Lett.* **2003**, *91*, 267204.
[84] M. Ognjanović, M. Radović, M. Mirković, Ž. Prijović, M. Del Puerto Morales, M. Čeh, S. Vranješ-Durić, B. Antić, *ACS Appl. Mater. Interfaces* **2019**, *11*, 41109.
[85] K. Nishimoto, S. Ota, G. Shi, R. Takeda, S. B. Trisnanto, T. Yamada, Y. Takemura, *AIP Adv.* **2019**, *9*, 035347.
[86] S. K. Shaw, A. Biswas, A. Gangwar, P. Maiti, C. L. Prajapat, S. S. Meena, N. K. Prasad, *J. Magn. Magn. Mater.* **2019**, *484*, 437.
[87] P. Bender, D. Honecker, L. Fernández Barquín, *Appl. Phys. Lett.* **2019**, *115*, 132406.
[88] P. Bender, E. Wetterskog, D. Honecker, J. Fock, C. Frandsen, C. Moerland, L. K. Bogart, O. Posth, W. Szczerba, H. Gavilán, R. Costo, M. T. Fernández-Díaz, D. González-Alonso, L. Fernández Barquín, C. Johansson, *Phys. Rev. B* **2018**, *98*, 224420.
[89] B. Faure, E. Wetterskog, K. Gunnarsson, E. Josten, R. P. Hermann, T. Brückel, J. W. Andreasen, F. Meneau, M. Meyer, A. Lyubartsev, L. Bergström, G. Salazar-Alvarez, P. Svedlindh, *Nanoscale* **2013**, *5*, 953.
[90] D. Serantes, D. Baldomir, C. Martinez-Boubeta, K. Simeonidis, M. Angelakeris, E. Natividad, M. Castro, A. Mediano, D. X. Chen, A. Sanchez, L. I. Balcells, B. Martínez, *J. Appl. Phys.* **2010**, *108*, 073918.
[91] A. Fernández-Pacheco, R. Streubel, O. Fruchart, R. Hertel, P. Fischer, R. P. Cowburn, *Nat. Commun.* **2017**, *8*, 15756.
[92] N. Daffé, F. Choueikani, S. Neveu, M. A. Arrio, A. Juhin, P. Ohresser, V. Dupuis, P. Sainctavit, *J. Magn. Magn. Mater.* **2018**, *460*, 243.
[93] P. Dutta, S. Pal, M. S. Seehra, N. Shah, G. P. Huffman, *J. Appl. Phys.* **2009**, *105*, 2007.
[94] J. Fock, L. K. Bogart, D. González-Alonso, J. I. Espeso, M. F. Hansen, M. Varón, C. Frandsen, Q. A. Pankhurst, *J. Phys. D Appl. Phys.* **2017**, *50*, 265005.
[95] M. Testa-Anta, M. A. Ramos-Docampo, M. Comesaña-Hermo, B. Rivas-Murias, V. Salgueiriño, *Nanoscale Adv.* **2019**, *1*, 2086.
[96] T. J. Daou, J.-M. Greneche, S.-J. Lee, S. Lee, C. Lefevre, S. Bégin-Colin, G. Pourroy, *J. Phys. Chem. C* **2010**, *114*, 8794.
[97] C. Phatak, A. K. Petford-Long, M. De Graef, *Curr. Opin. Solid State Mater. Sci.* **2016**, *20*, 107.
[98] I. V. Golosovsky, M. Tovar, U. Hoffman, I. Mirebeau, F. Fauth, D. A. Kurdyukov, Y. A. Kumzerov, *JETP Lett.* **2006**, *83*, 298.
[99] S. Mühlbauer, D. Honecker, É. A. Périgo, F. Bergner, S. Disch, A. Heinemann, S. Erokhin, D. Berkov, C. Leighton, M. R. Eskildsen, A. Michels, *Rev. Mod. Phys.* **2019**, *91*, 015004.
[100] A. Kovács, K. Sato, V. K. Lazarov, P. L. Galindo, T. J. Konno, Y. Hirotsu, *Phys. Rev. Lett.* **2009**, *103*, 115703.
[101] J. Curiale, M. Granada, H. E. Troiani, R. D. Sánchez, A. G. Leyva, P. Levy, K. Samwer, *Appl. Phys. Lett.* **2009**, *95*, 043106.
[102] T. N. Shendruk, R. D. Desautels, B. W. Southern, J. Van Lierop, *Nanotechnology* **2007**, *18*, 455704.
[103] R. J. Tackett, A. W. Bhuiya, C. E. Botez, *Nanotechnology* **2009**, *20*, 445705.
[104] S. Sharma, R. S. Ningthoujam, N. S. Gajbhiye, *Chem. Phys. Lett.* **2013**, *558*, 48.
[105] A. Kostopoulou, K. Brintakis, M. Vasilakaki, K. N. Trohidou, A. P. Douvalis, A. Lascialfari, L. Manna, A. Lappas, *Nanoscale* **2014**, *6*, 3764.
[106] J. M. Greneche, *Hyperfine Interact.* **2003**, *148–149*, 79.
[107] J. M. D. Coey, *Phys. Rev. Lett.* **1971**, *27*, 1140.
[108] R. H. Kodama, A. E. Berkowitz, E. J. Mc Niff, S. Foner, *Phys. Rev. Lett.* **1996**, *77*, 394.
[109] R. H. Kodama, A. E. Berkowitz, *Phys. Rev. B* **1999**, *59*, 6321.
[110] E. Tronc, P. Prené, J. P. Jolivet, J. L. Dormann, J. M. Grenèche, *Hyperfine Interact.* **1998**, *112*, 97.
[111] M. Varón, M. Beleggia, T. Kasama, R. J. Harrison, R. E. Dunin-Borkowski, V. F. Puntes, C. Frandsen, *Sci. Rep.* **2013**, *3*, 1234.
[112] C. Gatel, F. J. Bonilla, A. Meffre, E. Snoeck, B. Warot-Fonrose, B. Chaudret, L. M. Lacroix, T. Blon, *Nano Lett.* **2015**, *15*, 6952.
[113] S. Disch, E. Wetterskog, R. P. Hermann, A. Wiedenmann, U. Vainio, G. Salazar-Alvarez, L. Bergström, T. Brückel, *New J. Phys.* **2012**, *14*, 013025.
[114] K. L. Krycka, R. A. Booth, C. R. Hogg, Y. Ijiri, J. A. Borchers, W. C. Chen, S. M. Watson, M. Laver, T. R. Gentile, L. R. Dedon, S. Harris, J. J. Rhyne, S. A. Majetich, *Phys. Rev. Lett.* **2010**, *104*, 2.
[115] K. L. Krycka, J. A. Borchers, R. A. Booth, Y. Ijiri, K. Hasz, J. J. Rhyne, S. A. Majetich, *Phys. Rev. Lett.* **2014**, *113*, 147203.
[116] K. L. Krycka, J. A. Borchers, R. A. Booth, C. R. Hogg, Y. Ijiri, W. C. Chen, S. M. Watson, M. Laver, T. R. Gentile, S. Harris, L. R. Dedon, J. J. Rhyne, S. A. Majetich, *J. Appl. Phys.* **2010**, *107*, 09B525.
[117] D. Zákutná, D. Nižňanský, L. Barnsley, A. Feoktystov, D. Honecker, S. Disch, *Phys. Rev. X* **2020**, *10*, 031019.
[118] F. Sayed, N. Yaacoub, Y. Labaye, R. S. Hassan, G. Singh, P. A. Kumar, J. M. Greneche, R. Mathieu, G. C. Hadjipanayis, E. Agostinelli, D. Peddis, *J. Phys. Chem. C* **2018**, *122*, 7516.
[119] Y. Labaye, O. Crisan, L. Berger, J. M. Greneche, J. M. D. Coey, *J. Appl. Phys.* **2002**, *91*, 8715.
[120] M. Bersweiler, P. Bender, L. G. Vivas, M. Albino, M. Petrecca, S. Mühlbauer, S. Erokhin, D. Berkov, C. Sangregorio, A. Michels, *Phys. Rev. B* **2019**, *100*, 144434.
[121] S. D. Oberdick, A. Abdelgawad, C. Moya, S. Mesbahi-Vasey, D. Kepaptsoglou, V. K. Lazarov, R. F. L. Evans, D. Meilak, E. Skoropata, J. Van Lierop, I. Hunt-Isaak, H. Pan, Y. Ijiri, K. L. Krycka, J. A. Borchers, S. A. Majetich, *Sci. Rep.* **2018**, *8*, 3425.
[122] M. Herlitschke, S. Disch, I. Sergueev, K. Schlage, E. Wetterskog, L. Bergström, R. P. Hermann, *J. Phys. Conf. Ser.* **2016**, *711*, 012002.
[123] B. Pacakova, S. Kubickova, G. Salas, A. R. Mantlikova, M. Marciello, M. P. Morales, D. Nižňanský, J. Vejpravova, *Nanoscale* **2017**, *9*, 5129.
[124] D. Carta, M. F. Casula, A. Falqui, D. Loche, G. Mountjoy, C. Sangregorio, A. Corrias, *J. Phys. Chem. C* **2009**, *113*, 8606.
[125] D. Carta, M. F. Casula, P. Floris, A. Falqui, G. Mountjoy, A. Boni, C. Sangregorio, A. Corrias, *Phys. Chem. Chem. Phys.* **2010**, *12*, 5074.
[126] A. Yang, C. N. Chinnasamy, J. M. Greneche, Y. Chen, S. D. Yoon, Z. Chen, K. Hsu, Z. Cai, K. Ziemer, C. Vittoria, V. G. Harris, *Nanotechnology* **2009**, *20*, 185704.
[127] H. L. Andersen, M. Saura-Múzquiz, C. Granados-Miralles, E. Canévet, N. Lock, M. Christensen, *Nanoscale* **2018**, *10*, 14902.
[128] H. L. Andersen, C. Granados-Miralles, M. Saura-Múzquiz, M. Stingaciu, J. Larsen, F. Søndergaard-Pedersen, J. V. Ahlburg, L. Keller, C. Frandsen, M. Christensen, *Mater. Chem. Front.* **2019**, *3*, 668.
[129] N. Fontaiña-Troitiño, M. A. Ramos-Docampo, M. Testa-Anta, B. Rodríguez-González, M. Bañobre-López, L. Bocher, K. P. McKenna, V. Salgueiriño, *J. Mater. Chem. C* **2018**, *6*, 12800.
[130] J. Rockenberger, E. C. Scher, A. P. Alivisatos, *J. Am. Chem. Soc.* **1999**, *121*, 11595.
[131] T. Hyeon, S. S. Lee, J. Park, Y. Chung, H. Bin Na, *J. Am. Chem. Soc.* **2001**, *123*, 12798.
[132] P. Guardia, J. Pérez-Juste, A. Labarta, X. Batlle, L. M. Liz-Marzán, *Chem. Commun.* **2010**, *46*, 6108.
[133] W. W. Yu, J. C. Falkner, C. T. Yavuz, V. L. Colvin, *Chem. Commun.* **2004**, 2306.

[134] F. X. Redl, C. T. Black, G. C. Papaefthymiou, R. L. Sandstrom, M. Yin, H. Zeng, C. B. Murray, S. P. O'Brien, *J. Am. Chem. Soc.* **2004**, *126*, 14583.
[135] J. Park, K. An, Y. Hwang, J.-G. Park, H.-J. Noh, J.-Y. Kim, J.-H. Park, N.-M. Hwang, T. Hyeon, *Nat. Mater.* **2004**, *3*, 891.
[136] Y. Wang, J. He, C. Liu, W. H. Chong, H. Chen, *Angew. Chem., Int. Ed.* **2015**, *54*, 2022.
[137] A. G. Roca, L. Gutiérrez, H. Gavilán, M. E. Fortes Brollo, S. Veintemillas-Verdaguer, M. del, P. Morales, *Adv. Drug Delivery Rev.* **2019**, *138*, 68.
[138] A. G. Roca, D. Nižňanský, J. Poltierova-Vejpravova, B. Bittova, M. A. González-Fernández, C. J. Serna, M. P. Morales, *J. Appl. Phys.* **2009**, *105*, 114309.
[139] P. Guardia, B. Batlle-Brugal, A. G. Roca, O. Iglesias, M. P. Morales, C. J. Serna, A. Labarta, X. Batlle, *J. Magn. Magn. Mater.* **2007**, *316*, e756.
[140] A. Shavel, B. Rodríguez-González, M. Spasova, M. Farle, L. M. Liz-Marzán, *Adv. Funct. Mater.* **2007**, *17*, 3870.
[141] A. Lak, M. Kraken, F. Ludwig, A. Kornowski, D. Eberbeck, S. Sievers, F. J. Litterst, H. Weller, M. Schilling, *Nanoscale* **2013**, *5*, 12286.
[142] M. Levy, A. Quarta, A. Espinosa, A. Figuerola, C. Wilhelm, M. García-Hernández, A. Genovese, A. Falqui, D. Alloyeau, R. Buonsanti, P. D. Cozzoli, M. A. García, F. Gazeau, T. Pellegrino, *Chem. Mater.* **2011**, *23*, 4170.
[143] A. Walter, C. Billotey, A. Garofalo, C. Ulhaq-Bouillet, C. Lefèvre, J. Taleb, S. Laurent, L. Vander Elst, R. N. Muller, L. Lartigue, F. Gazeau, D. Felder-Flesch, S. Begin-Colin, *Chem. Mater.* **2014**, *26*, 5252.
[144] P. Torruella, R. Arenal, F. De La Peña, Z. Saghi, L. Yedra, A. Eljarrat, L. López-Conesa, M. Estrader, A. López-Ortega, G. Salazar-Alvarez, J. Nogués, C. Ducati, P. A. Midgley, F. Peiró, S. Estradé, *Nano Lett.* **2016**, *16*, 5068.
[145] R. Chen, M. G. Christiansen, A. Sourakov, A. Mohr, Y. Matsumoto, S. Okada, A. Jasanoff, P. Anikeeva, *Nano Lett.* **2016**, *16*, 1345.
[146] S. J. Kemp, R. M. Ferguson, A. P. Khandhar, K. M. Krishnan, *RSC Adv.* **2016**, *6*, 77452.
[147] M. Unni, A. M. Uhl, S. Savliwala, B. H. Savitzky, R. Dhavalikar, N. Garraud, D. P. Arnold, L. F. Kourkoutis, J. S. Andrew, C. Rinaldi, *ACS Nano* **2017**, *11*, 2284.
[148] C. Pereira, A. M. Pereira, C. Fernandes, M. Rocha, R. Mendes, M. P. Fernández-García, A. Guedes, P. B. Tavares, J. M. Grenéche, J. P. Araújo, C. Freire, *Chem. Mater.* **2012**, *24*, 1496.
[149] D. Kim, N. Lee, M. Park, B. H. Kim, K. An, T. Hyeon, *J. Am. Chem. Soc.* **2009**, *131*, 454.
[150] M. V. Kovalenko, M. I. Bodnarchuk, R. T. Lechner, G. Hesser, F. Schäfler, W. Heiss, *J. Am. Chem. Soc.* **2007**, *129*, 6352.
[151] H. Gavilán, E. H. Sánchez, M. E. F. Brollo, L. Asín, K. K. Moerner, C. Frandsen, F. J. Lázaro, C. J. Serna, S. Veintemillas-Verdaguer, M. P. Morales, L. Gutiérrez, *ACS Omega* **2017**, *2*, 7172.
[152] A. Lak, T. Kahmann, S. J. Schaper, J. Obel, F. Ludwig, P. Müller-Buschbaum, J. Lipfert, *ACS Appl. Mater. Interfaces* **2020**, *12*, 217.
[153] X. Sun, N. F. Huls, A. Sigdel, S. Sun, *Nano Lett.* **2012**, *12*, 246.
[154] M. Estrader, A. López-Ortega, I. V. Golosovsky, S. Estradé, A. G. Roca, G. Salazar-Alvarez, L. López-Conesa, D. Tobia, E. Winkler, J. D. Ardisson, W. A. A. Macedo, A. Morphis, M. Vasilakaki, K. N. Trohidou, A. Gukasov, I. Mirebeau, O. L. Makarova, R. D. Zysler, F. Peiró, M. D. Baró, L. Bergström, J. Nogués, *Nanoscale* **2015**, *7*, 3002.
[155] A. Lak, D. Niculaes, G. C. Anyfantis, G. Bertoni, M. J. Barthel, S. Marras, M. Cassani, S. Nitti, A. Athanassiou, C. Giannini, T. Pellegrino, *Sci. Rep.* **2016**, *6*, 33295.
[156] J.-H. Lee, J.-T. Jang, J.-S. Choi, S. H. Moon, S.-H. Noh, J.-W. Kim, J.-G. Kim, I.-S. Kim, K. I. Park, J. Cheon, *Nat. Nanotechnol.* **2011**, *6*, 418.
[157] G. C. Lavorato, R. Das, Y. Xing, J. Robles, F. J. Litterst, E. Baggio-Saitovitch, M. H. Phan, H. Srikanth, *ACS Appl. Nano Mater.* **2020**, *3*, 1755.
[158] A. López-Ortega, M. Estrader, G. Salazar-Alvarez, A. G. Roca, J. Nogués, *Phys. Rep.* **2015**, *553*, 1.
[159] J. Nogués, J. Sort, V. Langlais, V. Skumryev, S. Suriñach, J. S. Muñoz, M. D. Baró, *Phys. Rep.* **2005**, *422*, 65.
[160] S. H. Noh, W. Na, J. T. Jang, J. H. Lee, E. J. Lee, S. H. Moon, Y. Lim, J. S. Shin, J. Cheon, *Nano Lett.* **2012**, *12*, 3716.
[161] S. H. Moon, S. H. Noh, J. H. Lee, T. H. Shin, Y. Lim, J. Cheon, *Nano Lett.* **2017**, *17*, 800.
[162] K. Lee, S. Lee, B. Ahn, *Chem. Mater.* **2019**, *31*, 728.
[163] K. Sartori, F. Choueikani, A. Gloter, S. Begin-Colin, D. Taverna, B. P. Pichon, *J. Am. Chem. Soc.* **2019**, *141*, 9783.
[164] M. Vasilakaki, C. Binns, K. N. Trohidou, *Nanoscale* **2015**, *7*, 7753.
[165] M. Estrader, A. López-Ortega, S. Estradé, I. V. Golosovsky, G. Salazar-Alvarez, M. Vasilakaki, K. N. Trohidou, M. Varela, D. C. Stanley, M. Sinko, M. J. Pechan, D. J. Keavney, F. Peiró, S. Suriñach, M. D. Baró, J. Nogués, *Nat. Commun.* **2013**, *4*, 2960.
[166] M. Sytnyk, R. Kirchschlager, M. I. Bodnarchuk, D. Primetzhofer, D. Kriegner, H. Ennser, J. Stangl, P. Bauer, M. Voith, A. Hassel, F. Krumeich, F. Ludwig, A. Meingast, G. Kothleitner, M. V. Kovalenko, W. Heiss, *Nano Lett.* **2013**, *13*, 586.
[167] V. Mameli, A. Musinu, A. Ardu, G. Ennas, D. Peddis, D. Nižňanský, C. Sangregorio, C. Innocenti, N. T. K. Thanh, C. Cannas, *Nanoscale* **2016**, *8*, 10124.
[168] J. Jang, H. Nah, J.-H. Lee, S. H. Moon, M. G. Kim, J. Cheon, *Angew. Chem.* **2009**, *121*, 1260.
[169] L. Kumar, P. Kumar, V. Kuncser, S. Greculeasa, B. Sahoo, M. Kar, *Mater. Chem. Phys.* **2018**, *211*, 54.
[170] R. Kumar, M. Kar, *Ceram. Int.* **2016**, *42*, 6640.
[171] A. Simonov, A. L. Goodwin, *Nat. Rev. Chem.* **2020**, *4*, 657.
[172] R. Hufschmid, H. Arami, R. M. Ferguson, M. Gonzales, E. Teeman, L. N. Brush, N. D. Browning, K. M. Krishnan, *Nanoscale* **2015**, *7*, 11142.
[173] E. Y. Yu, M. Bishop, B. Zheng, R. M. Ferguson, A. P. Khandhar, S. J. Kemp, K. M. Krishnan, P. W. Goodwill, S. M. Conolly, *Nano Lett.* **2017**, *17*, 1648.
[174] I. Fernández-Barahona, L. Gutiérrez, S. Veintemillas-Verdaguer, J. Pellico, M. D. P. Morales, M. Catala, M. A. Del Pozo, J. Ruiz-Cabello, F. Herranz, *ACS Omega* **2019**, *4*, 2719.
[175] Y. Luengo, M. A. Roldan, M. Varela, F. Herranz, M. P. Morales, S. Veintemillas-Verdaguer, *J. Phys. Chem. C* **2019**, *123*, 7356.
[176] D. Kim, K. Shin, S. G. Kwon, T. Hyeon, *Adv. Mater.* **2018**, *30*, 1802309.

Aidin Lak received his Ph.D. in physics in 2013 from the Technical University of Braunschweig, Germany. He then moved to Genoa, Italy, to carry out a postdoctoral research in the group of Nanomaterials for Biomedical Applications at the Italian Institute of Technology. From 2018 to 2020, he was an Alexander von Humboldt Postdoctoral Fellow at Ludwig-Maximilians-University in Munich and since then he is a senior postdoctoral researcher at LMU, Munich. His research interests include synthesis, bio-functionalization, and characterization of hybrid magnetic nanostructures for biomedical diagnostics and therapeutics as well as understanding the underlying physics.

Sabrina Disch is an Emmy-Noether research group leader in the Department of Chemistry at Universität zu Köln, Germany. After obtaining her Ph.D. degree from Forschungszentrum Jülich/RWTH Aachen (Germany) in 2010, she was a postdoctoral fellow at the University of Oregon (USA) and Institut Laue-Langevin in Grenoble (France) before joining Universität zu Köln in 2014. Her research interests include the structure and magnetism of magnetic nanoparticles and self-organized nanostructures as studied using x-ray and polarized neutron scattering techniques.

Philipp Bender received his Ph.D. in physics in 2013 from the Saarland University (Germany). After working as a postdoctoral researcher at the Saarland University and the University of Cantabria (Santander, Spain), he has been at the University of Luxembourg since 2018. His research focuses on the application of magnetic nanoparticles for biomedicine and their characterization by magnetometry and magnetic small-angle neutron scattering.

